A Calibrated Force-Based Model for Mixed Traffic Simulation

Qianwen Chao, Pengfei Liu, Yi Han, Yingying Lin, Chaoneng Li, Qiguang Miao, *Senior Member, IEEE*, and Xiaogang Jin, *Member, IEEE*

Abstract—Virtual traffic benefits a variety of applications, including video games, traffic engineering, autonomous driving, and virtual reality. To date, traffic visualization via different simulation models can reconstruct detailed traffic flows. However, each specific behavior of vehicles is always described by establishing an independent control model. Moreover, mutual interactions between vehicles and other road users are rarely modeled in existing simulators. An all-in-one simulator that considers the complex behaviors of all potential road users in a realistic urban environment is urgently needed. In this work, we propose a novel, extensible, and microscopic method to build heterogeneous traffic simulation using the force-based concept. This force-based approach can accurately replicate the sophisticated behaviors of various road users and their interactions in a simple and unified manner. We calibrate the model parameters using real-world traffic trajectory data. The effectiveness of this approach is demonstrated through many simulation experiments, as well as comparisons to real-world traffic data and popular microscopic simulators for traffic animation.

Index Terms—Traffic simulation, simulator, detailed traffic flow, heterogeneous, social force

1 Introduction

In recent years, with the popularity of virtual reality and autonomous driving, high-fidelity traffic simulators have become an effective tool that can provide various traffic conditions for virtual city generation and autonomous vehicle testing prior to real-world road driving [1], [2], [3]. In a complex traffic environment, vehicles, pedestrians, and cyclists constitute three important road users. Indeed, they also posses inseparable relationships and complex interactions in the real world. Accurately simulating their respective behaviors and interactions in transportation networks is critical to the future development of urban environments and traffic safety. Consequently, there is an urgent need for a simulator that considers all potential road users in a realistic urban environment.

In the computer graphics community, vehicles and pedestrians have always been studied separately. A vast amount of literature exists on modeling and simulating traffic flows or pedestrian crowd dynamics, using either agent-based microscopic or continuum-based macroscopic methods [4], [5], [6]. However, all of the investigations were carried out under the assumption of ideal traffic environments. Modeling of non-ideal real-world traffic scenarios remains a less explored research topic. In addition, current existing traffic simulators (SUMO [7], SimMobility [8], and Vissim [9]) model the behaviors of vehicles, pedestrians, bicycles, and their interactions discretely. Furthermore, each specific behavior of each type of road user, such as vehicle acceleration, lane change, and interaction with pedestrians, is also modeled and controlled in different ways. Such non-unified approaches are complicated and inefficient in generating complex virtual traffic environments.

Recently, in the field of autonomous vehicle testing, some efforts have been made to generate powerful virtual mixed traffic scenarios. For example, the Apollo simulation platform [10] and Best *et al.*'s work [11] implement two non-vehicle traffic participants in simulation: pedestrians and cyclists. The behaviors of these non-vehicle road users, however, have been pre-defined and cannot react to vehicle motion in real time. The Carla simulator [12] introduces dynamic pedestrians into the simulation. However, the interaction between vehicle and pedestrian is handled in a simple predefined way: in an interaction, the pedestrian stops to wait for a few seconds to sense any vehicles, and then walks away without considering the existence of the vehicles. From this perspective, current existing simulators make decisions of autonomous vehicle movement in a reactive manner without considering mutual influences and real interactions between vehicles and other potential road users. As a consequence, creating a mixed simulation environment consisting of mutual influences and interactions

- *Qianwen Chao, Chaoneng Li, and Qiguang Miao are with the Department of Computer Science, Xidian University, Xi'an, Shaanxi 710038, China. E-mail: chaoqianwen15@gmail.com, xdchaonengli@163.com, qgmiao@mail.xidian.edu.cn.*
- *Pengfei Liu, Yi Han, Yingying Lin, and Xiaogang Jin are with the State Key Laboratory of CAD&CG, Zhejiang University, Hangzhou, Zhejiang 310058, China. E-mail: lpengfei@zju.edu.cn, hany28@mail2.sysu.edu.cn, missup109@163.com, jin@cad.zju.edu.cn.*

Manuscript received 11 January 2021; revised 28 October 2021; accepted 10 November 2021. Date of publication 16 November 2021; date of current version 31 January 2023.
The work of Xiaogang Jin was supported in part by the National Natural Science Foundation of China under Grant 62036010 and in part by the Key Research and Development Program of Zhejiang Province under Grant 2020C03096. Qiguang Miao was supported in part by the National Key R&D Program of China under Grant 2018YFC0807500, in part by the National Natural Science Foundations of China under Grants 61772396, 61772392, and 61902296, and in part by the Xian Key Laboratory of Big Data and Intelligent Vision under Grant 201805053ZD4CG37.
(Corresponding author: Qianwen Chao and Xiaogang Jin.)
Recommended for acceptance by J. Barbic.
Digital Object Identifier no. 10.1109/TVCG.2021.3128286

Fig. 1. Example of mixed traffic simulation result generated by our calibrated force-based approach.

among vehicles, two-wheelers, and pedestrians, is highly desired for autonomous vehicle testing.

In this paper, we focus on modeling heterogeneous traffic composed of various types of road users by a unified approach. We propose a simple, efficient, and scalable *force-based* framework to simulate the behaviors of vehicles, pedestrians, bicycles, and their interactions in a unified manner, in which any detailed behavior for each type of road user can be attributed to a specific force.

Specifically, there are several essential force terms in the presented method to model the behaviors of pedestrians, vehicles and bicycles: first, a term describing acceleration towards the desired velocity and movement target; second, a term reflecting that an agent maintains a certain distance from its neighboring agents; and third, a term describing an agent's relationship with static obstacles or lane boundaries for vehicles and bicycles to describe their lane-keeping behaviors. For vehicles and bicycles, an additional term modeling attractive effects is also requisite to simulate lane-changing behaviors. Moreover, interactions among different kinds of traffic agents are introduced as environmental feedback in the force form into their behavior control models. In order to make individual behavior in the simulation as realistic as that in real traffic, we calibrate the model parameters using traffic trajectory data obtained in the real world. Fig. 1 shows an example of mixed traffic simulation results generated by our calibrated force-based approach.

The main contributions of this work can be described as follows:

- It introduces a novel, scalable, calibrated approach based on the *force-based* concept to simulate complex virtual mixed traffic.
- Unlike previous traffic simulation methods, it introduces a unified model for various detailed behaviors of vehicles, including acceleration/deceleration, lane keeping, and lane changing behavior.
- It provides a viable solution for describing interactions among different types of road users in simulation.

2 Related Work

In this section, we first review previous related crowd simulation models and traffic synthesis methods. We then describe prior works on calibration of microscopic traffic models.

2.1 Crowd Simulation Methods

Agent-based crowd simulation models treat each person in the crowd as an intelligent agent with its own proprieties and goals. Each agent makes a decision individually from its neighborhood information for every time-step. Researchers have developed a variety of microscopic control models [13], including velocity-based and force-based models. In the velocity-based model, each agent selects a velocity by minimizing a given cost function. These methods include velocity obstacles (VO) and its several variants [14], [15], [16], [17], [18]. In the force-based model, each agent receives virtual forces generated from the spatial or social relationship between the agent and its neighbor. The Social Force Model (SFM) for pestrian dynamics by Helbing *et al.* [19], [20] are widely uses in the crowd simulation community.

In addition to the detailed modeling of crowd behaviors, there have been several attempts to introduce real captured crowd data into multi-agent simulation. By learning behavior patterns from real-world samples [21], [22], [23], [24], [25], [26], [27] and extracting real-world trajectories from videos, natural crowd behaviors can be synthesized [28], [29], [30], [31], [32].

Different from the above-mentioned crowd simulation methods that mainly focus on pedestrian crowd simulation, we are interested in developing a unified and scalable framework for mixed traffic simulation, and the framework is expected to be able to deal with the detailed complex interactions among vehicles, bicycles, and pedestrians.

2.2 Traffic Control Models

In traffic simulation, there are two kinds of widely-used traffic control models, based on the expression level of simulation details: continuum-based macroscopic models and agent-based microscopic models.

Macroscopic methods describe vehicles' behaviors and interactions at a low level of detail: a traffic stream is represented by a continuum, in terms of speed, flow, density, etc. [33], [34]. In the field of transportation, researchers have developed a number of macroscopic models, such as the well-known Lighthill-Whitham-Richards (LWR) model [35], [36], the Payne-Whitham (PW) model [37], [38] and the Aw-Rascle-Zhang (ARZ) model [39], [40]. In the field of computer graphics, Sewall *et al.* [41] extended the single-lane ARZ model to handle multi-lane traffic simulation by introducing a lane-changing model and utilizing a discrete visual representation for each vehicle. Wang *et al.* [42] focused on lane-changing behavior in flow-based continuum traffic simulations. In general, macroscopic methods are computationally efficient, but not suitable for simulating street-level traffic, which consists of rich interactions among individual cars.

In contrast, a microscopic model treats each vehicle as an autonomous agent, whose behavior is controlled based on instantaneous states of surrounding vehicles and road information. According to car-following principles [43], researchers have derived a variety of microscopic control models, including the optimal velocity model [44] and the intelligent driver model (IDM) [45]. Shen *et al.* [5] combined IDM with a flexible lane-changing model for urban traffic simulation. Chao *et al.* [6] modeled vehicles' interaction behaviors with pedestrians for mixed traffic simulation. The work of Garcia-

Dorado *et al.* [46] provided users with the flexibility to specify a desired vehicular traffic behavior to a road network. Microscopic methods can simulate complex vehicle behavior details, but only afford a limited scale of traffic due to their computational requirements. To address this issue, Sewall *et al.* [47] presented a hybrid traffic simulation model by integrating continuum- and agent-based methods to balance the trade-off between quality and efficiency at runtime.

2.3 Data-Driven Traffic Visualization and Simulation

With the development of advanced sensing hardware and computer vision techniques, empirical traffic flow datasets in the form of video, LiDAR, and GPS sensors are becoming increasingly available. Traffic visualization techniques based on existing data collections have also received notable attention in recent years. The works of Sewall *et al.* [48] and Wilkie *et al.* [49] reconstructed traffic flow from temporal-spatial data acquired by in-road sensors. In addition, researchers simulated the process of lane-changing in traffic simulation from a pre-collected vehicle trajectory dataset [4], or learned individual-specific driving characteristics from vehicle trajectory data extracted from driving video samples [50]. Recently, Li *et al.* [51] proposed a city-scale traffic simulation framework from mobile vehicle data (i.e., GPS traces) using statistical learning and metamodel-based optimization. Chao *et al.* [52] synthesized new vehicle trajectories through the combination of texture synthesis with microscopic traffic behavior rules, given a limited set of vehicle trajectories as the input samples. It is noteworthy that real-world traffic datasets from the Federal Highway Administration's Next Generation Simulation (NGSIM) [53] are used in the above works.

2.4 Traffic Model Calibration

The performance of traffic models largely depends on the parameter sets that they utilize to describe and control vehicle motion. Researchers have proposed several methods for calibrating traffic simulators with reference to real-world traffic data. During the model calibration process, the model parameters need to be adjusted until an acceptable match is identified between agent behavior in the simulation and that in the observed data.

Engineering judgment and trial-and-error methods remain widely employed, especially in industry [54]. More systematic approaches, including the gradient method [55] and the genetic algorithm [56], take the model calibration process as an optimization problem to solve: search for a combination of parameter values to minimize the objective function (usually an error term). Kesting and Triber calibrated and compared IDM and the Optimal Velocity model with the Bosch GmbH dataset using the genetic algorithm [57], [58].

3 Force-Based Framework

We present a two-layer force-based framework for hybrid traffic simulation, where the top layer separately calculates the detailed movement of each kind of road user, and the second layer describes the interaction between different road users, i.e., pedestrian-vehicle, pedestrian-bicycle, and bicycle-vehicle interaction. Inspired by the social force model [19], [20], [59], [60] for pedestrian dynamics, participants in mixed traffic behave as if they are driven by 'forces' of their desires, neighboring participants, and the surrounding environment (e.g., road structures, walls, or buildings). Assuming that individual i is an arbitrary road user in a mixed traffic flow, its movement can be determined by a combination of sociopsychological and physical forces. The total effect force $\mathbf{F}_i(t)$ is defined as follows

$$\mathbf{F}_i(t) = \mathbf{F}_i^0(t) + \sum_{j(\neq i)} \mathbf{F}_{ij}(t) + \sum_W \mathbf{F}_{iW}(t) + \sum_o \mathbf{F}_{io}(t) + \xi_i, \tag{1}$$

where the driving force $\mathbf{F}_i^0(t)$ reflects the individual's intention to move to a certain destination at a desired speed; the repulsive force $\mathbf{F}_{ij}(t)$ describes the effects of interactions with its neighboring individuals j; $\mathbf{F}_{iW}(t)$ measures the repulsive effects of the built environment W; $\mathbf{F}_{io}(t)$ is introduced to describe the interaction with other categories of road users; and ξ_i is a fluctuation term added to account for random variations.

The driving force $\mathbf{F}_i^0(t)$ describes individual i's motivation to move with an expected velocity $\mathbf{v}_i^0(t)$ by adapting the actual velocity $\mathbf{v}_i(t)$ within a certain relaxation time τ_i [20]

$$\mathbf{F}_i^0(t) = m_i \frac{\mathbf{v}_i^0(t) - \mathbf{v}_i(t)}{\tau_i} = m_i \frac{\mathbf{v}_i^0(t) - \mathbf{v}_i(t)}{\mathbf{v}_i^0(t)} \mathbf{a}_i, \tag{2}$$

where m_i is the mass of individual i; and $\mathbf{a}_i$ represents the desired acceleration.

In our framework, the repulsive force $\mathbf{F}_{ij}$ from a certain neighbor j is presented in different forms according to different characteristics of various kinds of road users. For pedestrians, this force is defined as a combination of social-psychological and physical forces, describing the psychological tendency of two pedestrians to move away from each other, and the physical contact force when they are in contact with each other. For motor vehicles, the repulsive force comes from all neighboring vehicles in sight within the current and adjacent lanes. For a specific neighboring motor vehicle j, the form of the force is designed differently depending on its located lane. For bicycles, this force is defined as a combination of the direct repulsive force for collision avoidance and the force for overtaking.

In mixed traffic scenarios, the environmental force $\mathbf{F}_{iW}$ describes constraints of the lane boundary W on individual i. For different types of road users, the influence of the built environment is analogous in form, but the magnitude of the force varies with the sensitivity of different types of individuals to distance

$$\mathbf{F}_{iW}(t) = U_i e^{\frac{\left|r_i^W + v_i^W T_i\right|}{R_i}} \mathbf{n}_i^W, \tag{3}$$

where R_i is the sensitivity coefficient of individual i to distance; U_i is the scale factor of the environmental force; r_i^W represents the distance between individual i and lane boundary W; $\mathbf{n}_i^W$ is the unit vector pointing from the nearest position of lane boundary axis to individual i; v_i^W means the velocity component in the direction of $\mathbf{n}_i^W$; and T_i is the reaction time.

We define the interaction force $\mathbf{F}_{io}(t)$ as the environmental influence, respectively, for the interactions between vehicles and pedestrians, vehicles and bicycles, and pedestrians and bicycles. Interacting individuals treat each other as environmental impacts and compute feedback on themselves. For vehicle-bicycle interactions, the form of the interaction force varies with different positional relationships between them. Vehicle-pedestrian and bicycle-pedestrian interactions take place at pedestrian crossings, which include the decision-making mechanism and the feedback-intrigued action process. It is worth noting that, as pedestrian behaviors are computed using the popular social force model [19], [20], we will focus on the force modeling of vehicles and bicycles, which will be elaborated in Section 4.

4 Forces for Behaviors in Mixed Traffic

4.1 Force-Based Model for Vehicles

For mixed traffic simulation, models should include as many complex traffic behaviors as possible, yet be computed in an efficient manner. However, in existing microscopic traffic simulators [5], [7], [8], [9], [45], [61], each specific behavior of vehicles, such as acceleration/deceleration and lane changing, is modeled and controlled one by one. In addition, these methods often focus on vehicle movement in the forward direction, but very limited efforts have been attempted on simulating vehicle dynamics in the lateral direction in traffic simulations, such as the influence from lane boundaries and neighboring vehicles in the field of view. Moreover, existing lane-changing models [62], [63], [64] in the intelligent transportation field only focus on the decision-making process of the vehicle lane-changing, but ignore the subsequent execution process of that maneuver.

To overcome these constraints, we propose a force-based simulation model for vehicles that uses forces to describe the vehicle's internal desires and its interactions with the external environment, thereby guiding the vehicle's behaviors by integrating the effects of various forces. The force terms are designed according to the characteristics of vehicle movements:

- Drivers mainly drive in a car-following mode. However, the vehicle's movement is also affected by all neighboring vehicles in the field of view.
- Drivers must keep driving within lane markings and adhere to traffic regulations.
- Drivers tend to change lanes to take advantage of the allowable speed in a target lane or to cope with some imperative factors, such as the end of the current lane.

4.1.1 Repulsive Forces Between Vehicles

When moving along a traffic flow, a vehicle c is subjected to repulsive forces from all neighboring vehicles within sight in its current and adjacent lanes. As illustrated in Fig. 2, due to the lane-keeping rules in traffic, the impact of the vehicle q in adjacent lanes on vehicle c is far less than that of the front vehicle p in the current lane, in the absence of lane changing. Therefore, we design the repulsive force $\mathbf{F}_{cj}$ from a certain neighbor j in different forms.

Influence from vehicles in adjacent lanes: The force from a neighboring vehicle q in the adjacent lane (blue vehicle in Fig. 2) is mainly associated with its distance and direction to vehicle c, defined as follows

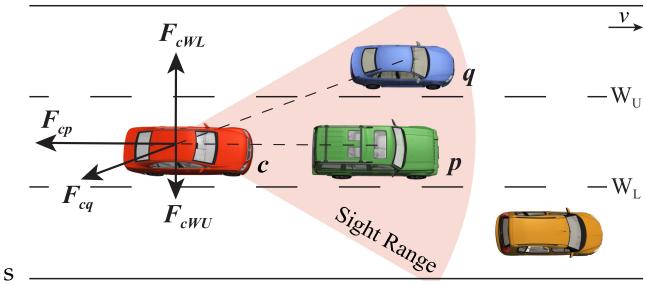

Fig. 2. The sight range (in the red sector) of a vehicle c, and its repulsive forces F_{cp} and F_{cq} from surrounding vehicles in the current and adjacent lanes. The environmental force F_i^W of two-side lane boundaries (W_U and W_L) is also shown here, denoted as F_{cW_U} and F_{cW_L}.

$$\mathbf{F}_{cq}^{n}(t) = U_c e^{-\frac{r_{cq}}{R_c}} \mathbf{n}_{cq}, \tag{4}$$

where U_c is the scale factor; R_c is the vehicle's sensitivity coefficient to distance; r_{cq} is the distance between vehicle q and c; and $\mathbf{n}_{cq}$ is the unit vector pointing from vehicle q's center to vehicle c's center.

Influence from the vehicle in the current lane: According to the car-following phenomenon [43] in real-world traffic, vehicle c's behavior in the current lane is mainly a response to its leading vehicle p (green vehicle in Fig. 2), for the purpose of maintaining a safe gap to vehicle p while seeking its desired velocity during driving. The intelligent driver model (IDM) [45] is a popular microscopic model to describe this car-following behavior, and has been well calibrated to demonstrate its performance using real-world trajectory data [57]. Therefore, we utilize the braking deceleration term in IDM to approximate the repulsive force $\mathbf{F}_{cp}^{f}$ of vehicle c from its leading vehicle p. Specifically, force $\mathbf{F}_{cp}^{f}$ can be defined as a function of vehicle c's velocity v_c, its bumper-to-bumper distance s, and relative velocity Δv to leading vehicle p

$$\mathbf{F}_{cp}^{f}(t) = -b_c \left(\frac{s^*}{s}\right)^2 \mathbf{n}_c, \tag{5}$$

$$s^* = s_c^0 + v_c T_c + \frac{v_c \Delta v}{2\sqrt{a_c b_c}}, \tag{6}$$

where the parameters (a_c, b_c, s_c^0, T_c) are constant for each vehicle, which describe its basic driving capability; a_c and b_c are, respectively, vehicle c's maximum acceleration and comfortable deceleration; s_c^0 is jam space headway; T_c is the desired safety time headway; and $\mathbf{n}_c$ is the unit vector denoting the current direction of vehicle c's movement. The repulsive force $\mathbf{F}_{cp}^{f}$ is not only related to the gap distance between the two vehicles, but also to the velocity difference between the two and the speed of the current vehicle. This can ensure that when the speed difference between two vehicles is large, the current vehicle will be subjected to a greater repulsive force, thus avoiding the occurrence of sudden braking as the two vehicles are too close to each other. Moreover, incorporating vehicle c's current velocity v_c and the driver's reaction time T_c can guarantee that the safety distance is maintained at a relatively high speed.

4.1.2 Force for Lane Changing

A vehicle generally performs lane changing if it can go faster in a target lane. According to the lane-changing model proposed by Kesting *et al.* [61], the incentive condition for a lane-changing decision of vehicle c is fulfilled if the utility of a possible lane change for motor vehicle c is larger than the influence on the involved neighbors (the original follower o in the original lane, and the new follower n in a target lane), which is typically measured in acceleration values

$$\tilde{a}_c - a_c + \lambda_c(\tilde{a}_n - a_n + \tilde{a}_o - a_o) > \Delta a_c^{th}, \tag{7}$$

where the first two terms refer to the acceleration gain of a possible lane changing for vehicle c and the other terms indicate the acceleration loss of the original and new followers; $\tilde{a}_c$ denotes the new acceleration for vehicle c after a prospective lane change; and a_c denotes its acceleration prior to the lane change. The politeness factor λ_c determines to which degree these successors influence the lane-changing decision of vehicle c. Δa_c^{th} is the lane-changing threshold which prevents lane changes for marginal advantage [5].

If the incentive criterion (Eq. 7) is satisfied, the lane changing is performed by introducing an attraction force $\mathbf{F}_c^{cl}$ from the target lane to vehicle c. Since the attraction force is to counteract the lane-keeping constraint from the current lane boundary, $\mathbf{F}_c^{cl}$ can be computed akin to the environmental force $\mathbf{F}_{cW}$ from current lane boundaries, using Eq. 3.

4.2 Force-Based Model for Bicycles

Similar to the simulation control model of vehicles and pedestrians, the behavior of bicycles in a mixed traffic flow can also be described by employing the *force-based* concept. However, unlike the ways in which pedestrians and vehicles interact with their neighbors, bicyclists possess their own characteristics when interacting with neighbors. First, bicycles generally do not move in a car-following manner, and utilize lateral space to a greater extent than do motor vehicles. Second, unlike pedestrians, bicyclists tend to adjust their motions, rather than completely stop and wait when an event occurs, in order to reduce the amount of required physical exertion.

Therefore, we describe a bicycle k's repulsive force $\mathbf{F}_{kj}$ from its neighbor j with two force components: the direct repulsive force $\mathbf{F}_{kj}^R$ for collision avoidance and the force $\mathbf{F}_{kj}^E$ for overtaking

$$\mathbf{F}_{kj}(t) = \mathbf{F}_{kj}^R(t) + \phi_k(t)\mathbf{F}_{kj}^E(t), \tag{8}$$

$$\phi_k(t) = \begin{cases} 1, \tilde{r}_{kj} \le d_k^E \\ 0, \tilde{r}_{kj} > d_k^E \end{cases} \tag{9}$$

where $\phi_k(t)$ is a discriminant function; $\tilde{r}_{kj}$ is the horizontal distance between bicycle k and j; and d_k^E is the distance threshold for overtaking.

The direct repulsive force $\mathbf{F}_{kj}^R$ for collision avoidance is used to describe a cyclist's conscious response to avoid collisions with other bicycles nearby. In accordance with a bicycle's shape, we use an ellipse to define a bicycle's safety space in a certain period of time, and use the semi-minor axis of the ellipse to measure the degree of other bicycles' influence. As shown in Fig. 3, B is the semi-minor axis of the ellipse, and the relative velocity $(\Delta\mathbf{v} = \mathbf{v}_k - \mathbf{v}_j)$ of bicycle k to j lies on the semi-major axis of the ellipse. The position of bicycle k is the focus of the ellipse, and the neighboring bicycle j is located on the circumference of the ellipse. A smaller B means a shorter distance between bicycle k and j, which results in a larger repulsive force $\mathbf{F}_{kj}^R$. Formally, the force can be computed as follows

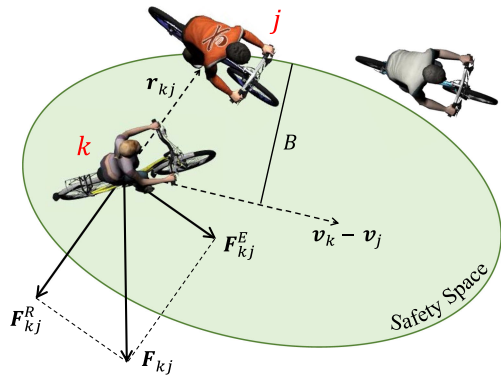

Fig. 3. Bicycle k's repulsive forces from its neighbor bicycle j. The green ellipse area denotes the safety space of bicycle k. The bicycle k's repulsive force $\mathbf{F}_{kj}$ from its neighbor j can be decomposed into two force components: one direct repulsive force $\mathbf{F}_{kj}^R$ for collision avoidance, and one force $\mathbf{F}_{kj}^E$ perpendicular to it for overtaking.

$$\mathbf{F}_{kj}^R(t) = U_k e^{-B/R_k}\mathbf{n}_{kj}, \tag{10}$$

$$B = \frac{1}{2}\sqrt{\left(\|\mathbf{r}_{kj}\| + \|\mathbf{r}_{kj} - \Delta\mathbf{v}\Delta t\|\right)^2 - (\|\Delta\mathbf{v}\Delta t\|)^2}, \tag{11}$$

where U_k and R_k represents the scale factor and the coefficient of sensitivity to distance, respectively; $\mathbf{r}_{kj}$ is the vector pointing from bicycle k to j; Δt is a time step; and $\mathbf{n}_{kj}$ is the unit vector from bicycle j to k.

At the same time, the overtaking force $\mathbf{F}_{kj}^E$ is introduced to describe bicycle k's flexible behavior when confronted with obstacles or congestion. The direction of $\mathbf{F}_{kj}^E$ is perpendicular to direct repulsive force $\mathbf{F}_{kj}^R$ and the magnitude is proportional to $\mathbf{F}_{kj}^R$

$$\mathbf{F}_{kj}^E(t) = \alpha_k \left\|\mathbf{F}_{kj}^R(t)\right\| \mathbf{n}_{kj}^V, \tag{12}$$

where $\mathbf{n}_{kj}^V$ is the unit vector perpendicular to $\mathbf{F}_{kj}^E$; and α_k is the scale factor.

4.3 Interactions in Mixed Traffic

In real-world traffic scenarios, pedestrians, bicycles, and vehicles have very complex interactions between each other. In some cities, there are no lanes designated for bicycle use; bicycles are supposed to move on either driveways or sidewalks. In other cases, even with bicycle lanes, some bicyclists prefer to ride in the lanes of other road users. On the other hand, pedestrians crossing a road while neglecting traffic signals is a common problem globally. In this section, we model vehicle-bicycle interactions, bicycle-pedestrian interactions, and interactions between vehicles and pedestrians crossing a road. In keeping with our *force-based* framework for each kind of road user, the mutual influences of the involved interacting individuals are measured in terms of forces and encoded as environmental feedback into their own behavioral control models.

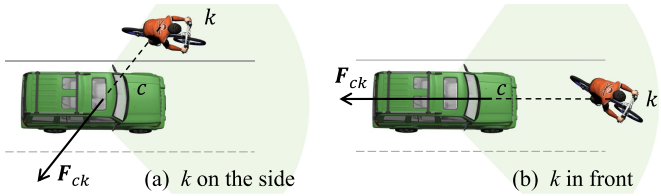

Fig. 4. Vehicle c receives repulsive force $\mathbf{F}_{ck}$ from bicycle k in an interaction.

4.3.1 Vehicle-Bicycle Interactions

To model vehicle-bicycle interactions, the interaction force is designed to take one of two different forms, depending on the positional relationship between bicycle k and vehicle c (see Fig. 4).

For vehicle c, if there is a side-by-side bicycle k in the sight range (the light green area), it will receive a lateral force from k for collision avoidance (Fig. 4a). However, if bicycle k is traveling in the near front, vehicle c will receive a rearward force for deceleration (Fig. 4b). Accordingly, vehicle c's interaction force $\mathbf{F}_{ck}$ from bicycle k is defined as

$$\mathbf{F}_{ck}(t) = \begin{cases} U_c e^{-\frac{s_c}{R_c}} \mathbf{n}_{ck}, & k \text{ by side} \\ -b_c * \left(\frac{s_c^0 + v_c T_c}{s_{ck}}\right)^2 \mathbf{n}_c, & k \text{ in front} \end{cases} \tag{13}$$

where s_{ck} denotes the distance between vehicle c and bicycle k; v_c is the velocity of the vehicle; $\mathbf{n}_{ck}$ is the unit vector pointing from bicycle k to vehicle c; and $\mathbf{n}_c$ represents the moving direction of vehicle c. U_c and R_c are the same factors in Eq. 4. The constant parameters (b_c, T_c, s_0) describe vehicle c's basic driving capability, which have the same meanings as those in Eq. 5.

Correspondingly, the interaction force $\mathbf{F}_{kc}$ subjected on bicycle k can take one of two different forms, depending on the positional relationship between k and c: whether the vehicle is on the side or in front. The force is formulated akin to Eq. 13.

4.3.2 Interactions With a Road-Crossing Pedestrian

A pedestrian is interaction with vehicles is conducted per lane. He or she perceives the surrounding traffic conditions, and the approaching vehicles correspond to his or her stimuli. Based on this perception, pedestrian i makes a walk-or-wait decision based on gap acceptance [65], [66] to judge whether the current distance gap between him or her and the approaching vehicle c can ensure a safe crossing. Both the pedestrian's predicted crossing time t_i and the vehicle's estimated passing time t_c are computed. The crossing is considered as safe if t_i is less than t_c. Otherwise, the pedestrian needs to wait for the next longer gap.

When pedestrian i is walking, the mutual influence between the pedestrian and the involved vehicle is quantified in terms of forces, and is incorporated into their original behavior control model as environmental feedback to drive their motions. Pedestrian i usually slows down at the beginning of crossing due to concerns about vehicle c's arrival time, and after successfully cutting in, the pedestrian tends to accelerate significantly due to the psychological impact of wanting to leave the danger zone. Inspired by Steven's psychophysical power law [67], we model this kind of dynamic behavior pattern, and compute the interaction force $\mathbf{F}_{ic}$ received by pedestrian i from vehicle c as follows

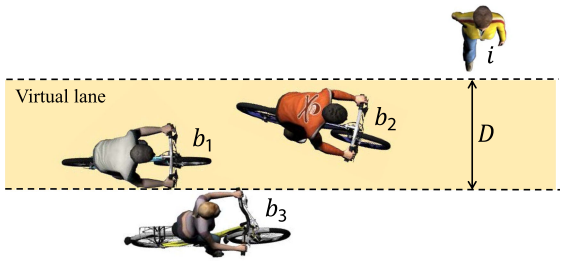

Fig. 5. Illustrative relationship between a pedestrian and the involved bicycles.

$$\mathbf{F}_{ic}(t) = \beta_i s_{ic}^{0.67} \mathbf{n}_{ic}, \tag{14}$$

where β_i is a scale factor; s_{ic} is the distance between pedestrian i and vehicle c; and $\mathbf{n}_{ic}$ is the unit vector pointing from c to i.

When facing a pedestrian i trying to cross a road, vehicle c tends to decelerate for safety. This situation is similar to the sudden crossing of a bicycle, as depicted in Fig. 4b. Therefore, we calculate the interaction force $\mathbf{F}_{ci}$ received by vehicle c from pedestrian i similarly as $\mathbf{F}_{ck}$ in Eq. 13.

4.3.3 Pedestrian-Bicycle Interaction

Mutual interactions that are similar to those described above also occur when pedestrian i cuts into the bicycle lane and interacts with bicycle b. The pedestrian has to make a walk-or-wait decision based on a safety judging criterion. If walking, the mutual feedback of the pedestrian and the involved bicycles is computed.

Unlike pedestrian-vehicle interaction, however, a pedestrian needs to consider interactions with multiple bicycles, because bicycles are more flexible than vehicles and always move side by side in a very short distance. Here, we define a "virtual lane" for a pedestrian's accurate gap-acceptance judgment and walk-or-wait decision making. As shown in Fig. 5, the virtual lane is constructed with a width of D and pedestrian i's current position as the starting boundary. In the decision-making process, the pedestrian i considers all bicycles in the virtual lane (b_1 and b_2 in Fig. 5). For each bicycle, compute pedestrian i's estimated crossing time t_i and bicycle b's predicted passing time t_b. The computation method is similar to that used in the pedestrian-vehicle interaction process. Then, the bicycle b with the smallest value of $\frac{t_i}{t_b}$ will be treated as the current interaction agent to have an interaction with pedestrian i. After pedestrian i has passed bicycle b, the virtual lane needs to be reconstructed, and a new round of decision making is initiated.

When crossing, pedestrian i is affected by the force of bicycle b, and the form of the force is similar to that in the pedestrian-vehicle interaction (Eq. 14).

At the same time, bicycle b's movement would be affected by pedestrians in the field of vision. When a moving pedestrian i appears in front of, and close to the bicycle, the cyclist would assess whether a collision would occur by calculating the relative velocity v_{bi} between them. To emulate this judgment, we first simplify the bicycle to an eclipse (see Fig. 6) with forward velocity of v_b, and then construct a

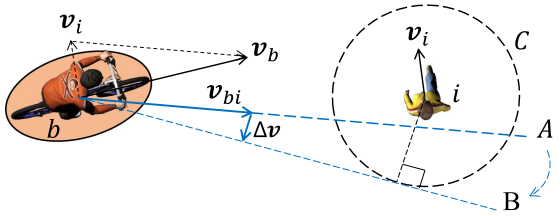

Fig. 6. Collision judgment of a bicycle b with its front pedestrian i.

circle C with the center of pedestrian i, the radius equal to the semi-major axis of the bicycle b, and the forward velocity of v_i. Subsequently, we draw a dashed line A extending from the bicycle, and taking the vector of relative velocity v_{bi} as the direction. If there is no intersection between the dashed line and the circle, it is considered as no collision, and bicycle b's movement would not be affected by pedestrian i. Conversely, collisions may occur if there is an intersection between A and C. The cyclist will gradually change the moving direction to avoid a collision with the pedestrian, while attempting to follow the original moving trajectory to the maximum extent until the dashed line is tangent to the circle, i.e., the dashed line A moves to B in Fig. 6. Accordingly, $\mathbf{\Delta v}$ denotes the minimum velocity change required for shifting the dashed line to be tangent to the circle. Based on this, we define a force $\mathbf{F}_{bi}$ subjecting on bicycle b from pedestrian i as follows

$$\mathbf{F}_{bi}(t) = \frac{\mathbf{\Delta v}}{T_i}, \tag{15}$$

where T_i is mentioned in Eq. 3.

On-Line Simulation. Up to now, the detailed behavior of each road user in a mixed traffic flow has been modeled by applying the described force-based method. Based on a given initial state (position and velocity) of each road user, our method can simulate sophisticated behaviors of various road users and their interactions. Taking into account the potentially complex environment required for virtual urban traffic simulation, more microscopic behaviors of arbitrary road users can be easily integrated into the current simulation framework by adding more specific forces. In addition, in order to make the simulation results more consistent with real-world traffic, we calibrate the proposed force-based model using real-world traffic trajectory data, which will be described in detail in Section 5.

5 Calibration

We use a heterogeneous traffic trajectory dataset provided by Apollo Scape [68] to calibrate the proposed model. The dataset was collected on urban streets using an Apollo acquisition car during rush hours, in which vehicles, pedestrians, and motorcycles/bicycles are detected and tracked (Fig. 7). Each individual's trajectory is recorded in a 1-min sequence at 2 fps intervals, containing the information of frame ID, object ID, object type, 3D position, length, width, height, orientation, speed, and acceleration. As a pre-processing step, the trajectory data are filtered by a Gaussian filter with a filter length of three to reduce the influence of noise on the model calibration performance.

Fig. 7. Visualization of real-world traffic trajectory data which are applied to calibration of our proposed force-based model.

Given the real-world traffic data, the calibration task is to determine the specific optimal parameter set of the force-based model that best fits the given trajectory for each traffic participant. Table 1 summarizes the model parameters that need to be calibrated and their empirical values. The calibration process can be formulated as an optimization problem, in which the model parameters need to be adjusted until an acceptable match is found between the simulated model dynamics and the observed agent behavior.

5.1 Objective Functions

For the optimization, an objective function is needed as a quantitative measure of the error between simulated behavior and observed behavior. Taking into account the dissimilar behavior patterns of different types of road users, we uniformly adopt the difference between the simulated position and the actual position as the error measure. Inspired by Chao *et al.*'s work on vehicle behavior diversification [50], we design the objective function using a mixed error metric as follows

$$F_{mix}[\mathbf{s}_{sim}] = \sqrt{\frac{1}{\langle|\mathbf{s}_{data}|\rangle}\left\langle\frac{|\mathbf{s}_{data}-\mathbf{s}_{sim}|^2}{|\mathbf{s}_{data}|}\right\rangle}, \tag{16}$$

TABLE 1
Parameters and Their Empirical Values for Our Calibration Process

Parameter	Value	Description
ξ_i	[2.0, 6.0]	fluctuation term for total effect force
a_i	[0, 35]	agent's desired acceleration
$\mathbf{v}_i^0$	[2.0, 6.0]	agent's optimal velocity
τ_i	[0.3, 10]	relaxation time for acceleration
U_i, U_c, U_k	[0.0, 1.0]	scale factor of force
R_i, R_c, R_k	[0.0, 1.0]	sensitivity to distance
T_i	[0.5, 0.6]	agent's reaction time
a_c	[2.0, 3.5]	vehicle's maximum acceleration
b_c	[2.0, 3.5]	vehicle's comfortable deceleration
s_c^0	[1.5, 2.5]	vehicle's jam space headway
T_c	[1E-5, 5]	vehicle's desire safety time headway
Δa_c^{th}	[0.0, 3.0]	vehicle's lane changing threshold
λ_c	[0.0, 1.0]	vehicle's politeness in lane changing
d_k^E	[1E-5, 2.0]	distance threshold for bicycle's overtaking
α_k	[1E-5, 2.0]	scale factor of bicycle's overtaking force
β_i	[1E-5, 1.0]	scale factor in vehicle-pedestrian interaction

where $\mathbf{s}_{data}$ and $\mathbf{s}_{sim}$ are the directed segments, respectively, in real trajectory and simulated trajectory within one time-step. Operator $\langle\cdot\rangle$ represents the temporal average of a time series of duration ($1 \sim N$ frames in our implementation), expressed as

$$\langle|\mathbf{s}|\rangle = \frac{1}{N}\sum_{i=1}^{N}|\mathbf{s}_i|. \tag{17}$$

5.2 Optimization With Adaptive Genetic Algorithm

We employ an adaptive genetic algorithm (AGA) to search for the optimal parameter set of the force-based model for each road user using the given real-world traffic trajectory data. The algorithm can be implemented as an iterative procedure that consists of a constant-size population of individuals. Each individual in the population represents a possible solution to the optimization problem. The genetic algorithm attempts to find the best solution to the problem by genetically propagating the population of individuals. The pseudo-code description of AGA is given in *Algorithm* 1.

Algorithm 1. Adaptive Genetic Algorithm

Input: population size N, parameters' range set PRS.
$gen \leftarrow 1$
$P[gen] \leftarrow GenerateInitialPopulation(PRS, N)$
while terminating conditions are not met **do**
  Evaluate the fitness of each individual in $P[gen]$
  $S[gen] \leftarrow RWLSelection(P[N])$
  while $|S[gen]| \leq N$ **do**
    Select two individuals in $S[N]$
    Compute the crossover rate p_c
    $NP[gen] \leftarrow Crossover(S[gen], p_c)$
    Compute the mutation rate p_m
    $NP[gen] \leftarrow Mutation(NP[gen], p_m)$
    $P[gen+1] \leftarrow ElitistSelect(P[gen], NP[gen])$
  end while
  $gen \leftarrow gen + 1$
end while
return the optimal parameter set

The adaptive genetic algorithm consists of the following steps:

1) Generate the initial generation $P[1]$. Suppose that there are N individuals in each generation. In order to represent the n parameters to be calibrated in each individual, each individual is encoded into a binary string, where each parameter is initialized with the empirical value range PRS (listed in Table 1).
2) Calculate the fitness of each individual. According to the principle of survival-of-the-fittest in nature, individuals with higher fitness are more likely to be selected as candidates for the subsequent generation. For our problem, we map the objective function F_{mix} defined by Eq. 16 to the fitness function $F_{fitness}$, which is defined as

$$F_{fitness} = \frac{1}{1 + F_{mix}}, \tag{18}$$

(a) (b) (c)

Fig. 8. Examples of interactions between different road users in the generated mixed traffic scenario: (a) pedestrian-vehicle interaction, (b) bicycle-vehicle interaction, and (c) bicycle-pedestrian interaction.

3) Select candidates using the Roulette Wheel Selection Algorithm [50] to achieve survival-of-the-fittest. Basically, the algorithm replicates individuals with higher fitness and eliminates individuals with lower fitness.
4) Crossover and mutation. The crossover operator combines two individuals to produce a new individual, with the possibility that good solutions can produce better ones. Specifically, we use the two-point crossover method, in which the operator randomly selects two crossover points in the binary string, and then interchanges the two binary strings between these points to generate two new individuals. After this, the mutation is used to achieve genetic diversity by altering one or more bit values in binary strings.
5) Retain the most elite individuals of the current generation to the next generation. Since the operators in Step 4 are random, the best-fitted individuals may be destroyed during the process. To avoid this situation, an elitist retention strategy is introduced. Specifically, compare the best individual in the new population after Step 4 with the parent population in Step 3. If the fitness is higher, it indicates that the population has developed toward the optimal solution. Otherwise, the worst half of individuals of the new population will be replaced by the best half of the parent population.
6) Repeat 2, 3, 4, and 5 until the terminal conditions are met. The termination criterion is specified by a fixed error for at least a given number of generations, or reaching the maximum number of iterations.

Using the calibrated parameter set, we can simulate mixed traffic similar to the given real-world traffic data. Considering the various behavioral characteristics of road users in different cities, further fine-tuning can be employed based on the calibrated parameters to realistically simulate complex traffic behaviors in various scenarios.

It is worth noting that besides the AGA, other nonlinear optimization methods, such as Particle Swarm Optimization (PSO), Simulated Annealing (SA), a combination of genetic and greedy algorithms (GA+G) [69], and the Covariance Matrix Adaptation Evolution Strategy method (CMA-ES) for Automated Parameter Fitting [70], can also be employed for the model calibration process.

6 Simulation Results

To demonstrate our force-based simulation framework, we generate mixed traffic flow on a road without any traffic signs (Fig. 1). Fig. 8 shows snapshots of the representative interactions between different types of road users in our synthesized mixed traffic flow.

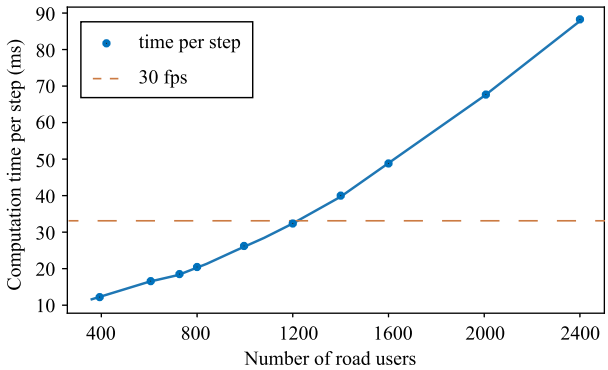

Fig. 9. Computation time per simulation step of our method.

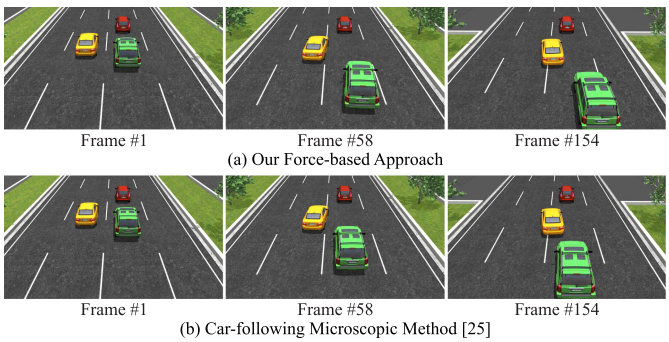

Fig. 10. Snapshots of a vehicle's (in green color) motions when a near-front vehicle (in yellow color) in the adjacent lane attempts to change lane ($58th$ frame), and soon afterwards moves back to its original lane due to the failure of lane changing ($154th$ frame). The motions of the green vehicles are computed using (a) the force-based approach proposed in this paper, and (b) the car-following microscopic method (IDM) [45].

Timing Performance. To determine the timing performance of our force-based simulation method, we conducted a series of experiments with different numbers of individuals in mixed traffic, in which the ratio of vehicles, bicycles, and pedestrians was 1:2:3. All of the timings were obtained with a 64-bit laptop machine with a 2.90 GHz Intel Core^{TM}I9-8950HK processor, 32 GB memory, and a Nvidia GeForce GTX 1080 video card. Fig. 9 illustrates the runtime performance of our method in terms of agent number. It can be seen that the computational costs scale approximately quadratic with the number of road users. Moreover, our approach can simulate approximately 1,200 agents in real time (30 fps) and 2500 agents at interactive rates (10 fps). The efficient time performance indicates that our approach can be straightforwardly plugged into various existing traffic simulation systems for autonomous vehicle testing and animation generation.

Interactions Between Vehicles. As shown in Fig. 10, we tested a green vehicle's response in a scenario in which a near-front yellow vehicle in the adjacent lane attempts to move into the green vehicle's lane. The yellow vehicle failed to change the lane and returned to its original lane. Fig. 10a shows the green vehicle's response through our force-based approach. At the $1st$ frame, both the green and yellow vehicles stayed in their original lanes. However, when the yellow vehicle tried to change its lane and get close to the green vehicle (at the $58th$ frame), the green vehicle attempted to avoid a collision in the lateral direction, owing to the repulsive force from the yellow vehicle (Eq. 4). Later, as the yellow vehicle failed to change its lane and returned to its original lane (at the $154th$ frame), the green vehicle moved back to the center of the current lane because of the repulsive force from lane boundaries. In order to evaluate the effectiveness of our force-based approach, we also computed the green vehicle's response in the same scenario using the Intelligent Driver Model (IDM) [45]. The model parameters for the green vehicle were set to empirical values [5]. Fig. 10b shows the corresponding simulation results. It is observed that the green vehicle only responded to the red vehicle in front in the same lane, and was not responsive to the yellow vehicle in the adjacent lane due to the car-following rules.

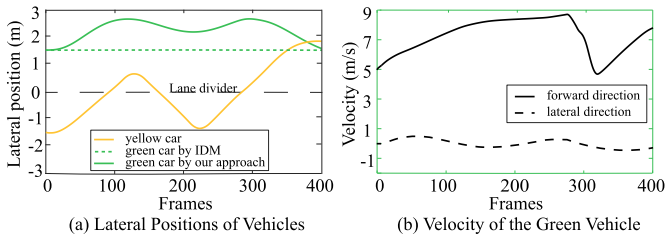

Fig. 11. (a) The lateral positions of the green vehicle and yellow vehicle; and (b) the velocity of the green vehicle in the forward direction (solid line) and in the lateral direction (dotted line) when the near-front yellow vehicle in the adjacent lane attempted to move into the green vehicle's lane.

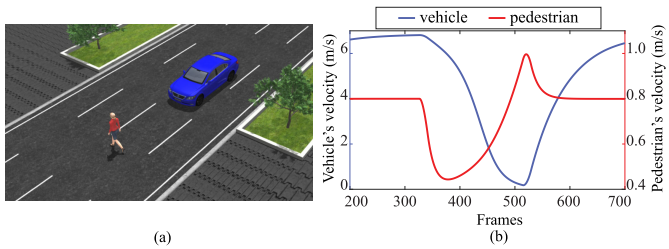

Fig. 12. (a) A snapshot of the interaction between a vehicle and a road-crossing pedestrian, and (b) the velocities of the pedestrian and vehicle during the interaction.

To better elucidate the performance of our approach, in Fig. 11, we show the lateral positional relationship between the green vehicle and yellow vehicle, and also list the velocity response of the green vehicle. The time period between the $211th$ and $400th$ frames shows that the yellow vehicle tried to change the lane again and successfully switched to the green vehicle's lane. An obvious lateral avoidance behavior of the green vehicle is observed during lane switching of the yellow vehicle. As soon as the yellow vehicle successfully cut in and became the leading vehicle of the green one (near the $280th$ frame), the green vehicle's force obtained from the yellow vehicle changed from Eq. 4 to Eq. 5, which triggered the green vehicle's emergency braking behavior (sudden velocity decrease in Fig. 11b) due to the sudden decrease in the gap between it and the preceding vehicle.

Interaction With Road-Crossing Pedestrians. Fig. 12a shows the snapshot of an interaction between a vehicle and a road-crossing pedestrian through our force-based approach. Fig. 12b shows the velocities of both the pedestrian (red line) and the vehicle (blue line). It is observed that both the vehicle and the pedestrian slowed down when they sensed

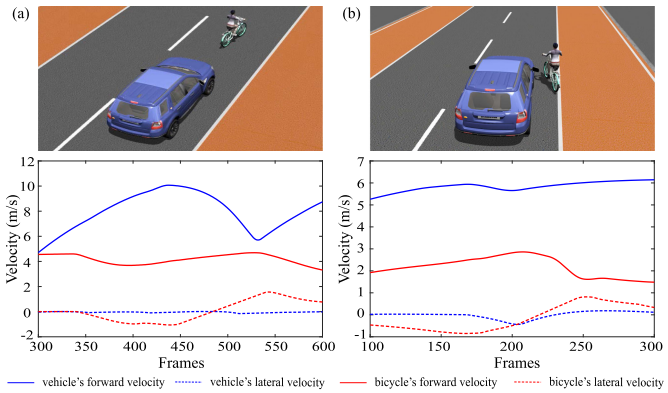

Fig. 13. The snapshots for two kinds of bicycle-vehicle interaction scenarios, and the velocities of both the cyclist and vehicle in their interaction process: (a) the cyclist riding in front of the vehicle; and (b) the cyclist riding near the side of the vehicle.

each other to ensure safety. Subsequently, after the vehicle continuously decelerated, the pedestrian accelerated to cross the lane as quickly as possible. Finally, both of them recovered to their original status after the interaction. Overall, the above analysis demonstrates that our force-based approach models the pedestrian-vehicle interactions in a realistic and smooth manner.

Bicycle-Vehicle Interactions. In Fig. 13, we show the snapshots of bicycle-vehicle interactions in two different situations described in Section 4.3.1: (a) a cyclist riding in front of a vehicle, and (b) a cyclist riding near the side of a vehicle. For each case, we also present the velocities of both the bicycle and the vehicle for comparison. The solid lines represent the velocities in the forward moving direction, and the dashed lines indicate those in the lateral direction. As can be seen from Fig. 13, when the bicycle was riding in the near front of the vehicle (from approximately $430th$ to $530th$ frame), the vehicle decelerated significantly in the forward direction, and its lateral movement did not change significantly. In contrast, when the bicycle was traveling near one side of the vehicle (from approximately $170th$ to $205th$ frame), the vehicle obviously avoided a collision with the bicycle in the lateral direction of movement. At the same time, there was a slight deceleration in the forward moving direction of the vehicle. It is worth noting that, in both interaction situations, while the vehicle was reacting, the bicycle also accelerated away from their interaction area and returned to its lane. As depicted in Fig. 13, there was apparent acceleration behavior in both directions of bicycle movement.

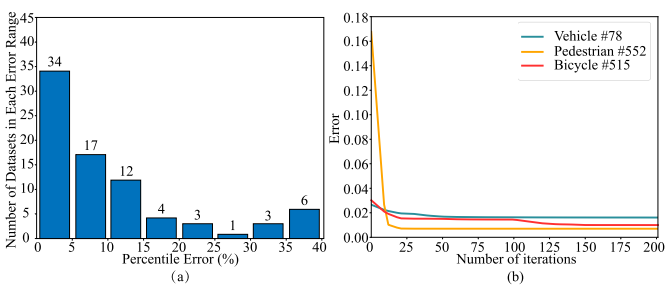

Fig. 14. (a) The learning mixed error F_{mix} distribution of the AGA algorithm and (b) the convergence performance for different types of road users (vehicle #78, pedestrian #552, and bicycle #515).

TABLE 2
Calibrated Parameter Values by AGA Algorithm

Parameter	vehicle #78	pedestrian #552	bicycle #515
ξ_i	2.31	4.12	1.83
a_i	5.0	1.0	4.0
$\mathbf{v}_i^0$	6.75	1.59	2.03
τ_i	2.70	0.63	0.97
U_i, U_c, U_k	1.00	0.23	0.74
R_i, R_c, R_k	7.80	6.41	7.99
T_i	2.73	0.63	0.97
a_c	5.0	-	-
b_c	2.9	-	-
s_c^0	3.95	-	-
T_c	2.72	-	-
Δa_c^{th}	0.62	-	-
λ_c	0.01	-	-
d_k^E	1.44	0.99	4.96
α_k	0.015	0.027	0.06
β_i	0.018	0.035	-

Performance of Model Calibration. We randomly select 80 road users (20 vehicles, 20 bicycles, and 40 pedestrians) from the Apollo Scape trajectory dataset to test the performance of our calibration algorithm. Here, we set the maximum number of generations to 500, with 100 individuals per generation. We define convergence as maintaining within a fixed error for at least 100 generations. The obtained error is defined in the range of $[0\%, 30\%]$, which is consistent with typical error ranges obtained in the previous studies of model calibration [50], [57]. Fig. 14a shows the resulting error distribution. Among the 80 tested individuals, 71 of them result in an error rate of less than 30%, whereas only 9 tested individuals lead to an error of 30% to 40%. The results show that using the calibrated parameters, the simulated behaviors of most individuals approximate the real trajectories with an acceptable error rate.

For detailed illustration, we randomly select an agent in each kind of road user (vehicle #78, pedestrian #552, and bicycle #515) to test the performance of our calibration algorithm. In Fig. 14b, we plot how the mixed error defined in Eq. 16 decreases over iterations. As shown in this figure, the errors of the above three types of traffic agents decrease dramatically in the first 50 generations, and then all converge within 200 iterations. It is worth noting that the curve of bicycle #515 (red line) falls into a temporary convergence during the $25th{\sim}100th$ generations, and then achieves further convergence at approximately the $150th$ generation. This proves that the AGA algorithm has the ability to avoid local optima.

Table 2 gives the specific calibrated value of each parameter. We apply these to the force-based model to reconstruct the behaviors of vehicle #78, pedestrian #552, and bicycle #515, and compare the simulated dynamics of these road users with their empirically measured values in Fig. 15. The yellow curves represent measured data, and the green curves represent simulated data. Fig. $15(a \sim c)$ show the comparison of trajectory. It can be seen that the green curve of each traffic individual is basically close to the corresponding yellow curve, which indicates that the objective function used for model calibration works well. Fig. $15(d \sim f)$ show the comparison results of velocity. It can be seen that the

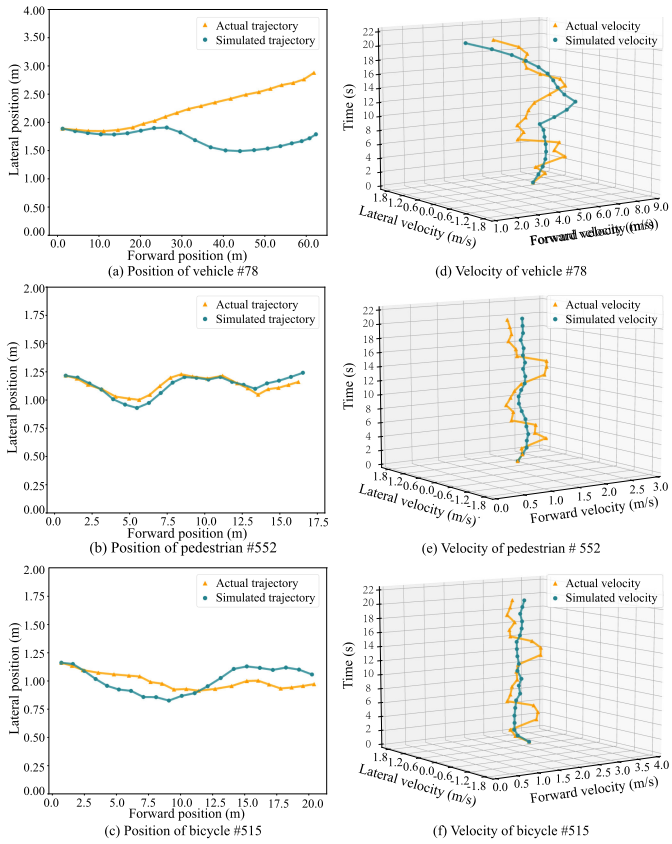

Fig. 15. Comparison of simulated and actual trajectories of vehicle #78 (left), pedestrian #552 (middle), and bicycle #515 (right). Figure $(a \sim c)$ shows the trajectory difference, while figure $(d \sim f)$ displays the velocity. The yellow curve represents actual data, and the green curve represents simulated data.

velocity difference between the yellow and green curves has been automatically reduced while optimizing with respect to trajectory. Overall, the tests in Fig. 15 validated that our calibrated force-based model can realistically simulate heterogeneous traffic in the real world.

Performance of Different Calibration Methods. In addition to AGA, we also tested four other optimization algorithms [69] for comparing the mixed error between simulated behavior and observed behavior (defined in Eq. 16). These four optimization algorithms are: Greedy Algorithm (G), Genetic Algorithm (GA), Simulated Annealing (SA), and Covariance Matrix Adaptation Evolution Strategy (CMA-ES). In our implementation, all these methods are calibrated on the same trajectory dataset for fair comparison. For each method, the approximate calibration time on the trajectory dataset is: 2.3 hours for CMA-ES, 8.1 hours for AGA, 8.3 hours for GA, 12.6 hours for SA, and 20.4 hours for G. Fig. 16 shows the error distributions of all optimization algorithms. After parameter calibration, the error of most agents can be reduced to less than 10%. Except for SA, other methods have no obvious difference in error. The error of AGA is slightly lower than other methods, and most errors of AGA are below 4%. Therefore, we employ AGA in our implementation. The errors of CMA-ES and GA are slightly higher than that of AGA, where CMA-ES costs less calibration time and GA takes similar calibration time as AGA. The Greedy algorithm (G) estimates parameters with a fixed precision using a brute force approach, and it obtains smaller errors at the cost of longer running time. Of all

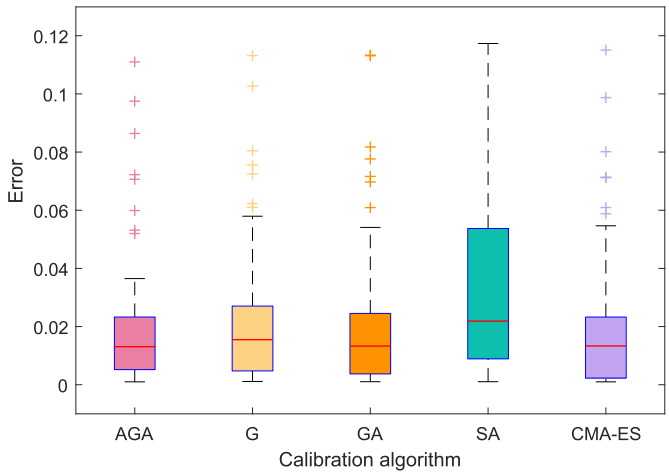

Fig. 16. Error distributions of different calibration algorithms.

five methods, SA has the worst performance because it is difficult to get out of the local optimum when there are many parameters (ranging from 16 to 20 in our experiments).

7 Conclusion and Discussion

In this paper, we proposed a calibrated force-based model that can approximately emulate intricate urban traffic. Pedestrians, bicycles, and vehicles are considered as the main road users. Their behaviors are encoded in a general, unified force-based framework, whose forces can be classified as the desire force to a target, repulsive forces with neighbors and the built environment, and interaction forces between different kinds of road users. The model parameters are calibrated to reconstruct heterogeneous traffic in the real world. Our approach offers a simple, efficient, and extensible method to simulate the different behavioral characteristics of different road users and realistic interaction effects in complex urban traffic environments. Experimental results were conducted to validate the performance of our approach by comparison with real-world traffic trajectories.

To the best of our knowledge, our model is the first unified and scalable framework for heterogeneous behaviors in mixed traffic scenarios. In previous crowd simulation methods, velocity-based methods are developed to address the local collision avoidance problem between multiple agents, while planning-based methods are mainly designed to deal with the global navigation problem. It is quite difficult to use these kinds of methods to describe the complex interactions between different types of road users. In contrast, purely data-driven methods use real-world traffic trajectory data as a reference and can capture more details of individual behavior. However, obtaining specific individual simulated behaviors through fine tuning is not user friendly. In addition, realistic simulation results rely on a large amount of various real-world data. However, data collection for mixed traffic is still a challenging and costly task. Different from the above methods, our force-based framework is unified and scalable by attributing any detailed behavior of each type of agent to a specific force. In order to simulate large-scale realistic mixed traffic in real time, we are also interested in developing a hybrid solution that combines our force-based method with a fast continuum model.

Although the simulation results are promising, the approach presented in this paper remains preliminary and can be improved in several aspects. First, it would be worthwhile to model the personalized behavioral characteristics of pedestrians, bicyclists, and drivers to generate heterogeneous traffic behaviors, thereby generating more realistic simulations. Second, for pedestrian crossing scenarios, a pedestrian's decision-making process is far more complex in real-world traffic than that in our current model [71]. In addition to the gap acceptance criterion, there are possibly other factors that need to be considered in making walk-or-wait decisions, such as the total number of pedestrians crossing the road together and waiting time. Third, different individual behaviors in the current framework are defined by different force formulas. We are interested in simplifying the current model, i.e., all forces are represented in the same form, but with different parameters to indicate different forces. Fourth, although we focus on the local interactions of various road users, other factors such as dynamic global route planning in a dynamically changing environment, and the heterogeneous traffic behaviors in an intersection scene with traffic signals, can also be incorporated into the simulation framework.

REFERENCES

[1] M. Aeberhard *et al.*, "Experience, results and lessons learned from automated driving on germany's highways," *IEEE Intell. Transp. Syst. Mag.*, vol. 7, no. 1, pp. 42–57, 2015.

[2] S. J. Anderson, S. C. Peters, T. E. Pilutti, and K. Iagnemma, "Design and development of an optimal-control-based framework for trajectory planning, threat assessment, and semi-autonomous control of passenger vehicles in hazard avoidance scenarios," in *Proc. Robot. Res.*, 2011, pp. 39–54.

[3] M. Likhachev and D. Ferguson, "Planning long dynamically feasible maneuvers for autonomous vehicles," *Int. J. Robot. Res.*, vol. 28, no. 8, pp. 933–945, 2009.

[4] H. Bi, T. Mao, Z. Wang, and Z. Deng, "A data-driven model for lane-changing in traffic simulation," in *Proc. ACM SIGGRAPH/Eurograph. Symp. Comput. Animation*, 2016, pp. 149–158.

[5] J. Shen and X. Jin, "Detailed traffic animation for urban road networks," *Graph. Models*, vol. 74, no. 5, pp. 265–282, 2012.

[6] Q. Chao, Z. Deng, and X. Jin, "Vehicle–pedestrian interaction for mixed traffic simulation," *Comput. Animation Virtual Worlds*, vol. 26, no. 3–4, pp. 405–412, 2015.

[7] D. Krajzewicz, J. Erdmann, M. Behrisch, and L. Bieker, "Recent development and applications of SUMO - Simulation of Urban MObility," *Int. J. Adv. Syst. Meas.*, vol. 5, no. 3&4, pp. 128–138, Dec. 2012.

[8] M. Adnan *et al.*, "Simmobility: A multi-scale integrated agent-based simulation platform," in *Proc. 95th Annu Meeting Transp. Res. Board Forthcoming Transp. Res. Rec.*, 2016.

[9] "Vissim," 2018. [Online]. Available: http://vision-traffic.ptvgroup.com

[10] "Apollo simulation," 2018. [Online]. Available: http://apollo.auto/platform/simulation.html

[11] A. Best, S. Narang, L. Pasqualin, D. Barber, and D. Manocha, "Autonovi-sim: Autonomous vehicle simulation platform with weather, sensing, and traffic control," in *Proc. IEEE Conf. Comput. Vis. Pattern Recognit. Workshops*, 2018, pp. 1048–1056.

[12] A. Dosovitskiy, G. Ros, F. Codevilla, A. Lopez, and V. Koltun, "CARLA: An open urban driving simulator," in *Proc. 1st Annu. Conf. Robot Learn.*, 2017, pp. 1–16.

[13] N. Pelechano, J. M. Allbeck, M. Kapadia, and N. I. Badler, *Simulating Heterogeneous Crowds with Interactive Behaviors*. Natick, MA, USA: A. K. Peters, Ltd., 2016.

[14] J. Van den Berg , M. Lin, and D. Manocha, "Reciprocal velocity obstacles for real-time multi-agent navigation," in *Proc. IEEE Int. Conf. Robot. Autom.*, 2008, pp. 1928–1935.

[15] S. J. Guy *et al.*"Clearpath: Highly parallel collision avoidance for multi-agent simulation," in *Proc. ACM SIGGRAPH/Eurograph. Symp. Comput. Animation*, 2009, pp. 177–187.

[16] J. Ondřej, J. Pettré, A.-H. Olivier, and S. Donikian, "A synthetic-vision based steering approach for crowd simulation," *ACM Transac. Graph.*, vol. 29, no. 4, pp. 1–9, 2010.

[17] S. J. Guy, S. Curtis, M. C. Lin, and D. Manocha, "Least-effort trajectories lead to emergent crowd behaviors," *Phys. Rev. E*, vol. 85, no. 1, 2012, Art. no. 016110.

[18] S. J. Guy, S. Kim, M. C. Lin, and D. Manocha, "Simulating heterogeneous crowd behaviors using personality trait theory," in *Proc. ACM SIGGRAPH/Eurograph. Symp. Comput. Animation*, 2011, pp. 43–52.

[19] D. Helbing and P. Molnar, "Social force model for pedestrian dynamics," *Phys. Rev. E*, vol. 51, no. 5, 1995.

[20] D. Helbing, I. Farkas, and T. Vicsek, "Simulating dynamical features of escape panic," *Nature*, vol. 407, no. 6803, pp. 487–490, 2000.

[21] K. H. Lee, M. G. Choi, Q. Hong, and J. Lee, "Group behavior from video: A data-driven approach to crowd simulation," in *Proc. ACM SIGGRAPH/Eurograph. Symp. Comput. Animation*, 2007, pp. 109–118.

[22] J. Pettré, J. Ondřej, A.-H. Olivier, A. Cretual, and S. Donikian, "Experiment-based modeling, simulation and validation of interactions between virtual walkers," in *Proc. ACM SIGGRAPH/Eurograph. Symp. Comput. Animation*, 2009, pp. 189–198.

[23] S. Kim, A. Bera, A. Best, R. Chabra, and D. Manocha, "Interactive and adaptive data-driven crowd simulation," in *Proc. IEEE Virtual Reality*, 2016, pp. 29–38.

[24] M. Zhao, W. Cai, and S. J. Turner, "Clust: Simulating realistic crowd behaviour by mining pattern from crowd videos," *Comput. Graph. Forum*, vol. 37, no. 1, pp. 184–201, 2018.

[25] E. Ju, M. G. Choi, M. Park, J. Lee, K. H. Lee, and S. Takahashi, "Morphable crowds," *ACM Trans. Graph.*, vol. 29, no. 6, pp. 1–10, 2010.

[26] J. Lee, J. Won, and J. Lee, "Crowd simulation by deep reinforcement learning," in *Proc. 11th Annu. Int. Conf. Motion, Interac. Games*, 2018, pp. 1–7.

[27] J. Amirian, W. Van Toll , J.-B. Hayet, and J. Pettré, "Data-driven crowd simulation with generative adversarial networks," in *Proc. 32nd Int. Conf. Comput. Animation Social Agents*, 2019, pp. 7–10.

[28] A. Lerner, Y. Chrysanthou, and D. Lischinski, "Crowds by example," *Comput. Graph. Forum*, vol. 26, no. 3, pp. 655–664, 2007.

[29] B. Yersin, J. Maïm, J. Pettré, and D. Thalmann, "Crowd patches: Populating large-scale virtual environments for real-time applications," in *Proc. Symp. Interactive 3D Graph. Games*, 2009, pp. 207–214.

[30] Y. Li, M. Christie, O. Siret, R. Kulpa, and J. Pettré, "Cloning crowd motions," in *Proc. ACM SIGGRAPH/Eurograph. Symp. Comput. Animation*, 2012, pp. 201–210.

[31] M. Kim, Y. Hwang, K. Hyun, and J. Lee, "Tiling motion patches," in *Proc. ACM SIGGRAPH/Eurograph. Symp. Comput. Animation*, 2012, pp. 117–126.

[32] K. Jordao, J. Pettré, M. Christie, and M.-P. Cani, "Crowd sculpting: A space-time sculpting method for populating virtual environments," *Comput. Graph. Forum*, vol. 33, no. 2, pp. 351–360, 2014.

[33] J.-P. Lebacque, S. Mammar, and H. H. Salem, "Generic second order traffic flow modelling," *Transp. Traffic Theory*, vol. 2007, pp. 755–776, 2007.

[34] D. Ngoduy, "Multiclass first-order traffic model using stochastic fundamental diagrams," *Transportmetrica*, vol. 7, no. 2, pp. 111–125, 2011.

[35] M. J. Lighthill and G. B. Whitham, "On kinematic waves. ii. a theory of traffic flow on long crowded roads," *Proc. Roy. Soc. London A: Math., Phys. Eng. Sci.*, vol. 229, no. 1178, pp. 317–345, 1955.

[36] P. I. Richards, "Shock waves on the highway," *Operations Res.*, vol. 4, no. 1, pp. 42–51, 1956.

[37] H. J. Payne, "Model of freeway traffic and control," *Mathematical Models Public Syst.*, pp. 51–61, 1971.

[38] G. B. Whitham, *Linear and Nonlinear Waves*. Hoboken, NJ, USA: Wiley, 1974.

[39] A. Aw and M. Rascle, "Resurrection of "second order" models of traffic flow," *SIAM J. Appl. Math.*, vol. 60, no. 3, pp. 916–938, 2000.

[40] H. M. Zhang, "A non-equilibrium traffic model devoid of gas-like behavior," *Transp. Res. Part B: Methodological*, vol. 36, no. 3, pp. 275–290, 2002.

[41] J. Sewall, D. Wilkie, P. Merrell, and M. C. Lin, "Continuum traffic simulation," *Comput. Graph. Forum*, vol. 29, no. 2, pp. 439–448, 2010.

[42] H. Wang, T. Mao, and Z. Wang, "Modeling interactions in continuum traffic," in *Proc. IEEE Virtual Reality*, 2014, pp. 123–124.

[43] D. L. Gerlough, "Simulation of freeway traffic on a general-purpose discrete variable computer," Ph.D. Dissertation, Univ. California, Los Angeles, CA, USA, 1955.
[44] M. Bando, K. Hasebe, A. Nakayama, A. Shibata, and Y. Sugiyama, "Dynamical model of traffic congestion and numerical simulation," *Phys. Rev. E*, vol. 51, no. 2, pp. 1035–1042, 1995.
[45] M. Treiber and D. Helbing, "Microsimulations of freeway traffic including control measures," *at-Automatisierungstechnik*, vol. 49, no. 11, pp. 478–484, 2001.
[46] I. Garcia-Dorado , D. G Aliaga, and S. V Ukkusuri, "Designing large-scale interactive traffic animations for urban modeling," *Comput. Graph. Forum*, vol. 33, no. 2, pp. 411–420, 2014.
[47] J. Sewall, D. Wilkie, and M. C. Lin, "Interactive hybrid simulation of large-scale traffic," *ACM Trans. Graph.*, vol. 30, no. 6, p. 135, 2011.
[48] J. Sewall, J. Van Den Berg , M. Lin, and D. Manocha, "Virtualized traffic: Reconstructing traffic flows from discrete spatiotemporal data," *IEEE Trans. Vis. Comput. Graph.*, vol. 17, no. 1, pp. 26–37, Jan. 2011.
[49] D. Wilkie, J. Sewall, and M. Lin, "Flow reconstruction for data-driven traffic animation," *ACM Trans. Graph.*, vol. 32, no. 4, pp. 1–10, 2013.
[50] Q. Chao, J. Shen, and X. Jin, "Video-based personalized traffic learning," *Graph. Models*, vol. 75, no. 6, pp. 305–317, 2013.
[51] W. Li, D. Wolinski, and M. C. Lin, "City-scale traffic animation using statistical learning and metamodel-based optimization," *ACM Trans. Graph.*, vol. 36, no. 6, pp. 1–12, 2017.
[52] Q. Chao, Z. Deng, J. Ren, Q. Ye, and X. Jin, "Realistic data-driven traffic flow animation using texture synthesis," *IEEE Trans. Vis. Comput. Graph.*, vol. 24, no. 2, pp. 1167–1178, Feb. 2018.
[53] "Next generation simulation," 2017. [Online]. Available: https://ops.fhwa.dot.gov/traffican alysistools/ngsim.htm
[54] L. Chu, H. X. Liu, J.-S. Oh, and W. Recker, "A calibration procedure for microscopic traffic simulation," in *Proc. IEEE Int. Conf. Intell. Transp. Syst.*, 2003, pp. 1574–1579.
[55] J. Hourdakis, P. G. Michalopoulos, and J. Kottommannil, "Practical procedure for calibrating microscopic traffic simulation models," *Transp. Res. Rec.*, vol. 1852, no. 1, pp. 130–139, 2003.
[56] R.-L. Cheu, X. Jin, K.-C. Ng, Y.-L. Ng, and D. Srinivasan,, "Calibration of Fresim for singapore expressway using genetic algorithm," *J. Transp. Eng.*, vol. 124, no. 6, pp. 526–535, 1998.
[57] A. Kesting and M. Treiber, "Calibrating car-following models by using trajectory data: Methodological study," *Transp. Res. Rec.*, vol. 2088, no. 1, pp. 148–156, 2008.
[58] A. Kesting and M. Treiber, "Calibration of car-following models using floating car data," in *Proc. Traffic Granular Flow*, 2009, pp. 117–127.
[59] A. Alahi, K. Goel, V. Ramanathan, A. Robicquet, L. Fei-Fei , and S. Savarese, "Social LSTM: Human trajectory prediction in crowded spaces," in *Proc. IEEE Conf. Comput. Vis. Pattern Recognit.*, 2016, pp. 961–971.
[60] A. Cosgun, E. A. Sisbot, and H. I. Christensen, "Anticipatory robot path planning in human environments," in *Proc. 25th IEEE Int. Symp. Robot Hum. Interactive Commun, .*, 2016, pp. 562–569.
[61] A. Kesting, M. Treiber, and D. Helbing, "General lane-changing model mobil for car-following models," *Transp. Res. Rec.: J. Transp. Res. Board*, no. 1999, pp. 86–94, 2007.
[62] M. Rahman, M. Chowdhury, Y. Xie, and Y. He, "Review of microscopic lane-changing models and future research opportunities," *IEEE Trans. Intell. Transp. Syst.*, vol. 14, no. 4, pp. 1942–1956, Dec. 2013.
[63] T. Toledo, H. Koutsopoulos, and M. Ben-Akiva , "Modeling integrated lane-changing behavior," *Transp. Res. Rec.: J. Transp. Res. Board*, no. 1857, pp. 30–38, 2003.
[64] J. Erdmann, "Sumos lane-changing model," in *Modeling Mobility with Open Data*. Berlin, Germany: Springer, 2015, pp. 105–123.
[65] B. Wan and N. Rouphail, "Using arena for simulation of pedestrian crossing in roundabout areas," *Transp. Res. Rec.: J. Transp. Res. Board*, no. 1878, pp. 58–65, 2004.
[66] P. Koh and Y. Wong, "Gap acceptance of violators at signalised pedestrian crossings," *Accident Anal. Prevention*, vol. 62, pp. 178–185, 2014.
[67] S. Kim, S. J. Guy, D. Manocha, and M. C. Lin, "Interactive simulation of dynamic crowd behaviors using general adaptation syndrome theory," in *Proc. ACM SIGGRAPH Symp. Interactive 3D Graph. Games*, 2012, pp. 55–62.
[68] P. Wang, X. Huang, X. Cheng, D. Zhou, Q. Geng, and R. Yang, "The apolloscape open dataset for autonomous driving and its application," *IEEE Trans. Pattern Anal. Mach. Intell.*, vol. 42, no. 10, pp. 2702–2719, Oct. 2020.
[69] D. Wolinski, S. J. Guy, A.-H. Olivier, M. Lin, D. Manocha, and J. Pettré, "Parameter estimation and comparative evaluation of crowd simulations," *Comput. Graph. Forum*, vol. 33, no. 2, pp. 303–312, 2014.
[70] G. Berseth, M. Kapadia, B. Haworth, and P. Faloutsos, "Steerfit: Automated parameter fitting for steering algorithms," in *Simulating Heterogeneous Crowds with Interactive Behaviors*. BocaRaton, FL, USA: AK Peters/CRC Press, 2016, pp. 229–246.
[71] J. Ren, W. Xiang, Y. Xiao, R. Yang, D. Manocha, and X. Jin, "Heterosim: Heterogeneous multi-agent systems simulation by interactive data-driven optimization," *IEEE Trans. Vis. Comput. Graph.*, vol. 27, no. 3, pp. 1953–1966, Mar. 2021.

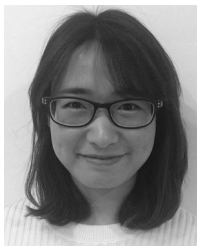

Qianwen Chao received the BSc degree in computer science from Xidian University in 2011and the PhD degree in computer science from the State Key Laboratory of CAD & CG, Zhejiang University, in 2016. She is currently a lecturer of computer science with Xidian University. Her research interests include crowd animation, cloth animation, and swarm micro-robotics.

Pengfei Liu received the bachelor's degree in software engineering from the North University of China in 2020. He is currently working toward the master's degree with the State Key Lab of CAD & CG, Zhejiang University. His research interests include crowd animation and traffic simulation.

Yi Han received the bachelor's degree in software engineering from Sun Yat-sen University in 2017. He is currently working toward the PhD degree with the State Key Laboratory of CAD & CG, Zhejiang University. His research interests include crowd animation and traffic simulation.

Yingying Lin received the bachelor's degreein 2017 in software engineering from the State Key Lab of CAD & CG, Zhejiang University, where she is currently working toward the master's degree. Her research interests include traffic simulation and virtual reality.

Chaoneng Li received the bachelor's degree in the Internet of Things from Northwest Normal University in 2017. He is working toward the PhD degree in computer science and technology with Xidian University. His research interests include computer vision and traffic prediction.

Qiguang Miao (Senior Member, IEEE) received the MEng and PhD degrees in computer science from Xidian University. He is currently a professor with the School of Computer Science, Xidian University. His research interests include intelligent information processing, intelligent image processing, and multi-scale geometric representations for image.

Xiaogang Jin (Member, IEEE) received the BSc degree in computer science, and the MSc and PhD degrees in applied mathematics from Zhejiang University, in 1989, 1992, and 1995, respectively. He is currently a professor with the State Key Laboratory of CAD & CG, Zhejiang University. His research interests include traffic simulation, collective behavior simulation, cloth animation, virtual try-on, digital face, implicit surface modeling and applications, creative modeling, computer-generated marbling, sketch-based modeling, and virtual reality. He was the recipient of ACM Recognition of Service Award in 2015 and Best Paper Awards from CASA 2017 and CASA 2018. He is a member of the ACM.